



Fragility curves of a slender structure fitted with tuned mass dampers subjected to turbulent wind and seismic loading

Curvas de fragilidad de una estructura esbelta equipada con amortiguadores de masa sintonizados sometidos a viento turbulento y carga sísmica

Pozos-Estrada Adrián

Instituto de Ingeniería, México

Ingeniería Estructural

E-mail: apozose@iingen.unam.mx

<https://orcid.org/0000-0002-6339-3388>

Martin del Campo-Preciado Jesús Osvaldo

Instituto de Ingeniería, México

Ingeniería Estructural

E-mail: JMartindelCampoP@iingen.unam.mx

<https://orcid.org/0000-0003-4049-1433>

Pozos-Estrada Oscar

Instituto de Ingeniería, México

Ingeniería Hidráulica

E-mail: opozose@iingen.unam.mx

<https://orcid.org/0009-0009-3549-557X>

Abstract

In the context of structural performance assessment, several studies have employed fragility curves and surfaces to evaluate the damage probability for predefined intensity levels of single or multiple hazards. Moreover, some of these studies have considered using tuned mass dampers (TMDs) to reduce the response of structures under wind or seismic loading. In this work, fragility curves and surfaces of a slender structure equipped with TMDs subjected to turbulent wind and seismic loading alone, as well as simultaneously, are developed. Simulated records for wind and earthquake ground motion are considered for the numerical analyses. For the development of fragility curves and surfaces, three damage states that account for the local and global behavior of the structure are considered. The analysis results indicate that, for the considered structure, a higher probability of damage is found from wind action than from earthquakes, and that an important reliability enhancement is achieved with the use of TMDs.

Keywords: Slender monument, fragility curves, fragility surfaces, wind hazard, seismic hazard, simultaneous hazard.

Resumen

En el contexto de la evaluación del desempeño estructural, varios estudios han empleado curvas y superficies de fragilidad para evaluar la probabilidad de daño para niveles de intensidad predefinidos de una o varias amenazas. Además, algunos de estos estudios han considerado el uso de amortiguadores de masa sintonizada (TMD, por sus siglas en inglés) para reducir la respuesta de las estructuras bajo cargas sísmicas o de viento. En este trabajo se desarrollan curvas y superficies de fragilidad de una estructura esbelta equipada con TMDs sometida a cargas sísmicas y de viento turbulento, sola y simultáneamente. Para los análisis numéricos se consideran registros simulados de movimiento del suelo y de velocidad de vientos turbulentos. Para el desarrollo de las curvas y superficies de fragilidad se consideran tres estados de daño que incluyen el comportamiento local y global de la estructura. Los resultados del análisis indican que, para la estructura considerada, se encuentra una mayor probabilidad de daño por acción del viento que por sismo, y que se logra una importante mejora de la confiabilidad con el uso de TMDs.

Descriptores: Monumento esbelta, curvas de fragilidad, superficies de fragilidad, peligro de viento, peligro sísmico, peligro simultáneo.

INTRODUCTION

The development of new materials and building techniques has allowed the construction of flexible structures with low structural damping. In most cases, such a type of engineered structures is located in places prone to different types of natural hazards. Examples of such kind of structures include high-rise buildings, towers, chimneys, and wind turbine towers (Wong & Harris, 2012; Zhou *et al.*, 2015; Li *et al.*, 2020; Jaimes *et al.*, 2020). To increase damping in this type of structures when they are subjected to diverse hazards, auxiliary damping devices, such as tuned mass dampers (TMDs), have been widely used to reduce their response (Pozos & Hong, 2015; Zhao *et al.*, 2018; Pozos & Gómez, 2019; Cui *et al.*, 2020; Zhang *et al.*, 2022).

In the context of structural performance assessment, several studies have employed fragility analysis to evaluate the probabilistic characterization of the demand concerning certain limit states by using fragility curves. The use of fragility functions is of paramount importance as they relate an intensity measure of a particular hazard, or hazards, with the probability of exceeding a predefined damage state. The use of fragility curves is vast, they have been widely applied to new and existing structures with different construction materials (e.g., concrete, steel, or composite). In the case of existing structures, fragility curves have been proposed to evaluate retrofitted structures, which can capture the impact on the structural system and not just individual elements (Padgett & DesRoches, 2009).

Most of the studies reported in the literature where fragility functions have been developed for different kinds of structures consider a single hazard (i.e., wind or earthquake), and only some include the combined effects of wind and earthquake. For example, Li *et al.* (2020) presented a multi-hazard fragility assessment of composite frame structures with buckling-restrained braces subjected to combined earthquake and wind. Zheng *et al.* (2019) carried out a damage risk assessment of a high-rise building against the multiple hazards of earthquake and strong wind with recorded data. Asareh *et al.* (2016) presented a multi-hazard fragility analysis, studying the variation of the probability of failure for earthquake intensity and wind action on the structure of a wind turbine. Martín del Campo & Pozos (2019) carried out a multi-hazard fragility analysis for a wind turbine support structure with an application to the Southwest of Mexico, a zone with high levels of wind and seismic hazard.

The study of structures with TMDs under multi-hazard effects has also been investigated by Zhao *et al.* (2018), where several ground motion records were

analyzed, as well as the effects of wind and waves with an experimental and numerical study of the structural response of a scaled offshore wind turbine with a TMD at the top of the model. More recently, Martín del Campo *et al.* (2021) developed fragility curves of land-based wind turbines with TMDs under cyclone and seismic loading. In their work, they found that equipping the studied structures with TMDs can imply a reduction greater than 50 % of the probability of reaching any of the studied damage states. From the studied cases, when the two hazards were considered to act simultaneously, the reduction in the probability of failure is (on average) 20 % less compared with the results from the single hazard cases.

Although the investigation of multi-hazard fragility assessment of structures with TMDs installed is not new, the development of fragility curves and the evaluation of the vulnerability of cultural infrastructure is scarce. Some examples of the evaluation of the structural behavior of cultural infrastructure include the vulnerability assessment for medieval civic towers in Italy (Casciati & Faravelli, 2008) and the performance evaluation of the monumental bridge Ponte delle Torri' in Spoleto, Italy (Gioffrè *et al.*, 2008). Furthermore, in recent years, Mexico has experienced an accelerated construction of tall and slender structures, which shows the need for studies to evaluate their behavior and performance under different type of actions (e.g., wind and seismic actions).

The main objective of this work is to develop fragility curves and surfaces of a slender monument fitted with TMDs subjected to turbulent wind and seismic loading in Mexico City, which is a city frequently struck by earthquakes from the coast of the Pacific Ocean and with important wind speeds that can cause damage to non-structural elements due to synoptic systems that converge along the Mexican territory (García *et al.*, 2012; Pozos *et al.*, 2014; Pozos-Estrada *et al.*, 2016). For the numerical analyses, the structure is subjected to the single and combined action of simulated seismic records and wind loading of different intensities. Fragility curves for the monument without and with TMDs under a single hazard and fragility surfaces for multiple hazards are developed. The effectiveness of the TMDs for increasing structural reliability is evaluated with an original criterion, which includes the use of curves and surfaces of reliability enhancement. The analysis results indicate that an important reliability enhancement is achieved with the use of TMDs, and that, for the structure considered, a higher probability of damage is found from wind action than from seismic action.

The present work is organized as follows: the wind- and seismic-induced response of the slender structure

without and with TMDs is presented in Section 2. Section 3 describes the development of fragility curves, followed by the analysis results which are presented in Section 4. The main observations of the study are presented in Section 5, where the conclusions are drawn.

WIND - AND SEISMIC - INDUCED RESPONSE OF THE SLENDER STRUCTURE WITHOUT AND WITH TMDs

DESCRIPTION OF THE STRUCTURE, STRUCTURE FITTED WITH TMDs AND MATHEMATICAL MODELING

The main structure of the monument is 117.58 m in height, with eight stainless-steel circular columns with 900 mm of diameter connected with steel elements along its height (Figure 1). The yielding stress of the steel elements is considered as 450 MPa. The structure supports a cladding system of 47 panels made of quartz plates. Each of the panels consists of 36 individual quartz plates with dimensions of 1475 mm width and 712.5 mm height, except one panel that consists of 48 individual quartz plates with similar dimensions as the others.

The structure was equipped with 10 TMDs. The TMD systems employed to mitigate the wind- and seismic-induced response comprise two separate assemblies: the system used to reduce the wind-induced response consists of eight identical units located inside the columns, and the system used to mitigate the seismic-induced response has two units with the same configuration. The TMD systems are composed of mass

blocks, springs connected to the mass blocks and the main structure, and a damping unit that includes a housing filled with a viscous fluid and a damper plunger, which can move horizontally. The vibrating masses are connected to a plate which is also connected to the plunger. Due to restrictions in space to install the TMD systems to reduce the wind-induced response alone, safety bars were employed to guarantee a vertical installation of them, together with a TMD frame and a supporting structure to connect the TMD system to the main structure. The supporting elements were designed to remain fixed, but the TMD systems can freely move in the horizontal direction. It is noted that the TMD systems are activated by the wind or earthquake-induced structural motion; the kinetic energy is transmitted from the structure to the TMD systems and is dissipated by means of the viscous dampers.

A three-dimensional finite element model of the structure was developed in ANSYS Parametric Design Language (APDL, 2019). For the modeling of the structure, a damping ratio equal to 1 % was used. Elements “COMBIN14” and “MASS21” were employed to model the TMDs systems. Figure 1a shows with red stars the locations where the effect of the TMD systems is applied to the main structure. The optimal parameters (*i.e.*, mass ratio (μ), frequency ratio (r_f), and ratio of damping of the TMD (ξ_d) used to characterize the TMD systems are summarized in Table 1. More details of the structure, the TMDs systems, and mathematical modeling can be found in Pozos & Gómez (2019).

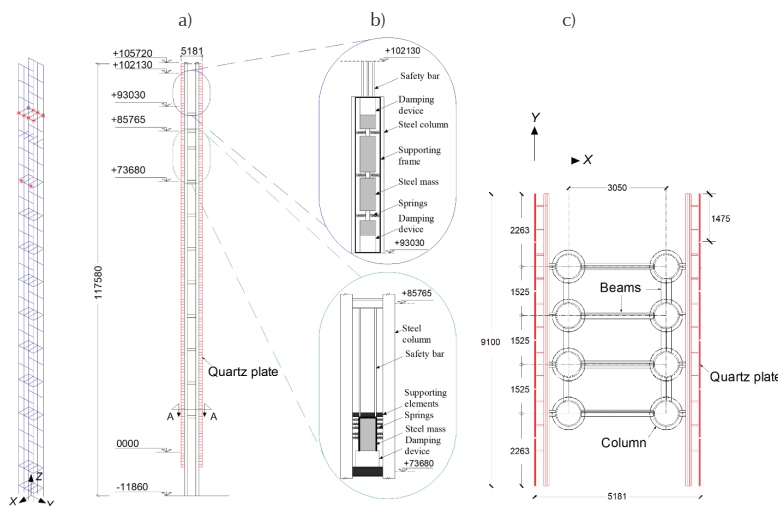


Figure 1. Structure of the monument: a) mathematical model; b) elevation view; c) detail A-A (all units in mm). The system for controlling wind-induced response is signaled in blue, whereas the system for control of the seismic-induced response is signaled in green

Table 1. Optimal TMD parameters used in the numerical analysis

Parameter	TMD system located at level +73680	TMD system located at level +102130
Mass ratio, μ	0.20	0.10
Frequency ratio, r_f	1.00	1.00
Ratio of damping of the TMDs, ξ_d	0.20	0.20

WIND AND SEISMIC MATHEMATICAL MODELING

The fragility analysis of the structure requires several excitation time histories, represented by both wind-speed and ground-motion signals. Although it is always desirable to employ real signals that represent the characteristics of these hazards at the site, such kind of signals are rarely available at any site. In that regard, the simulation of wind-speed and ground-motion records can be regarded as a feasible alternative, if such records represent the characteristics identified and reported in the literature concerning the hazards under analysis. In the present study, simulated wind-speed and ground-motion records at different intensities were performed to analyze the structure under such a range of intensities.

The dynamic analysis of the structure can be carried out in either the frequency domain or the time domain. We adopted the time-history approach since it allows a simple definition and characterization of the simulated time series and facilitates systematic analyses with the APDL code developed. Time-history analyses were performed on the structure to measure its response and the influence of the TMDs on it. All the analyses were carried out in the X-direction (Figure 1). Wind field simulations (i.e., wind-speed signals) were performed from the spectral representation method, based on the Power Spectral Density Function (PSDF) proposed by Kaimal *et al.* (1972). All the simulations consider a value for the turbulence intensity that varies with height according to the following equation:

$$I_u = d \left(\frac{z}{10} \right)^{-\alpha} \tag{1}$$

where d and α have been defined in accordance with wind-design standards for Mexico City for urban terrain (0.43 and 0.29, respectively, for terrain classification R4, according to NTC-DV (2017), acronym in Spanish). The length-scales of turbulence have been defined in accordance with ESDU (1975), these values can be applied in the Kaimal's turbulence spectrum for the simulations when proper scaling is performed.

The coherence function used for the turbulence co-spectra during the simulation of wind-speed signals is expressed from the exponential model, that can be used in conjunction with the Kaimal PSDF (Kaimal *et al.*, 1972):

$$\text{Coh}(n, r, U, L_u) = \exp \left(-12 \sqrt{\left(\frac{nr}{\langle U \rangle} \right)^2 + \left(\frac{0.12r}{\langle L_u \rangle} \right)^2} \right) \tag{2}$$

Where:

- n = frequency in Hz
- r = magnitude of the separation vector between two points in m

$\langle U \rangle$ and $\langle L_u \rangle$ have been computed as the average values of mean speed and length scale of turbulence in the along-wind direction for the two points, respectively.

For the computation of wind-induced loads a drag coefficient was considered on the structure. This coefficient $C_D = 2.879$ was estimated from the values proposed for bluff rectangular bodies in accordance with the Mexican standard MOC-DV (2020).

Values of mean wind speed within the range from 10 to 60 m/s at 10 m height (U_{10}) were considered for the simulations. The increments in wind intensity considered a step of 10 m/s, subsequent additional wind-field simulations were performed near the velocity intensities identified in the vicinity of the defined damage states for the fragility analysis (as described later, in Section Damage states definition). A total of 15 simulated wind fields were used for each intensity level, and the total length of each signal was 300 s. This number of simulations that were used is justified in an analysis of the variability of the structural response from the model, where the standard error seemed to remain unchanged with samples of at least 15 simulations. Figure 2 presents the comparison between some of the along-wind turbulence spectra from the simulated signals, at a height of 103.86 m for an intensity $U_{10} = 30$ m/s, and the analytical spectrum used.

For simplicity, the ground motions used on the analyses were simulated using the code based on random vibration theory SIMQKE (Vanmarcke & Gasparini, 1976); although advanced simulation techniques for ground motion records have been recently proposed in the literature (Hong & Liu, 2014; Liu & Hong, 2015; Hong & Liu, 2017; Hong & Cui, 2020). The SIMQKE program computes ground motion records from a user-defined response spectrum. The shape of the selected response spectra is in accordance with Mexico City earthquake-design regulations (NTC-DS, 2020, acronym in Spanish) for the site where the studied monument is located, and a fraction of 1 % the critical damping. The spectral periods of maximum pseudo acceleration in the objective response spectra correspond to the range between 0.8 and 1.5 s. The fundamental period of the site, according to NTC-DS (2020), is 1.1 s, far from the fundamental period of the structure in question, which is 4.17 s (Pozos & Gómez, 2019).

Due to the peculiar geotechnical conditions of the Valley of Mexico, earthquake ground motions in Mexi-

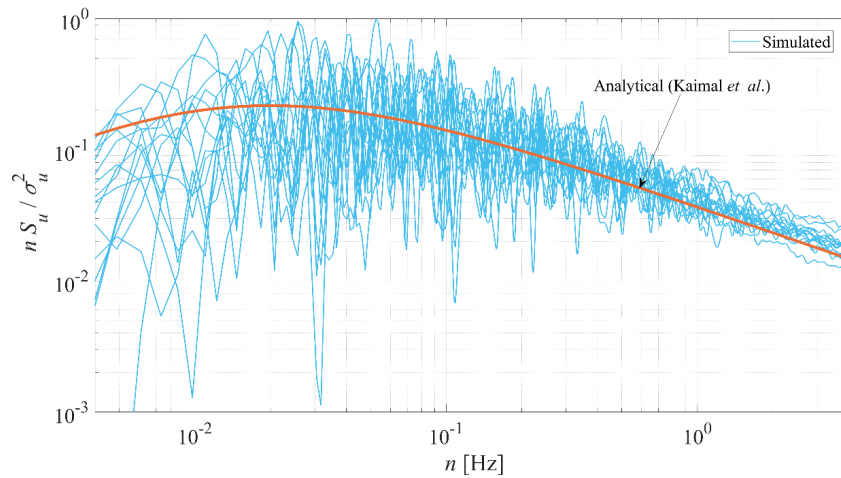


Figure 2. PSDFs of simulated wind signals

co City are distinguished for being of long duration. Thus, the simulated records assume a total duration of 200 s. The simulations were computed with a time-step of 0.05 s, as the wind-field simulations. The parameters used for the envelope of amplitude distribution in the simulated signals are as illustrated in Figure 3. The parameters used to simulate the ground motion records are consistent with the seismic records recorded at the Tacubaya station (2 km away from the structure), which is part of the seismic network of the national seismological service from Mexico.

The peak ground acceleration (PGA) was selected as measure to define the ground motion intensity for every simulation. Intensities covering from 0.1 to 1 g were simulated, with a total of 15 simulated records per intensity level (g represents the constant of gravitational acceleration). Similar to the criterion adopted for defining the number of wind-velocity signals, 15 simulations showed to be sufficient to observe no variation in the standard error from the structural response

analyzed from them. Figure 4 shows the response spectra from some of the simulated ground-motion records, for a value of PGA of 0.4 g. A fair match is seen between the simulations and the target spectrum.

DEVELOPMENT OF FRAGILITY CURVES

It is noted that the probability of damage could be assessed using the fragility curve in connection with the probability density functions (PDFs) of the IM (e.g., annual mean wind velocity and peak ground acceleration); however, for the characterization of the PDFs of annual wind velocities or peak ground acceleration, a complete catalogue of historic information of both hazards for Mexico City is required. Unfortunately, this information is not available and for this reason the evaluation of fragility curves on the structure was performed according to the criteria described in the following paragraphs.

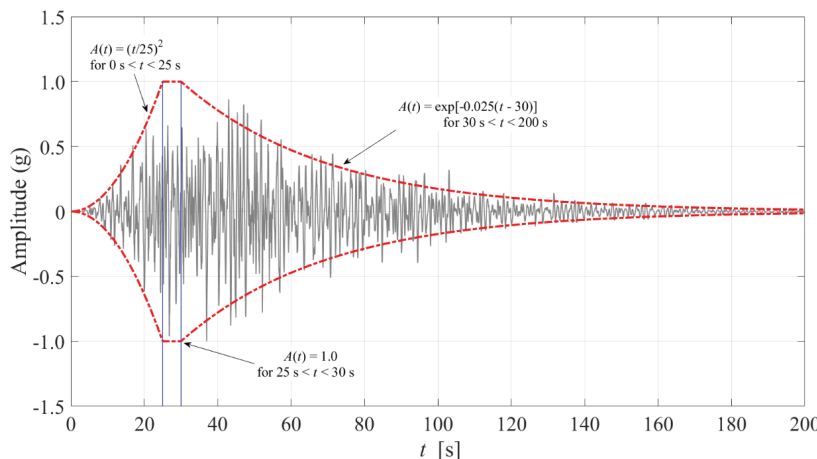


Figure 3. Amplitude time-distribution from simulated records

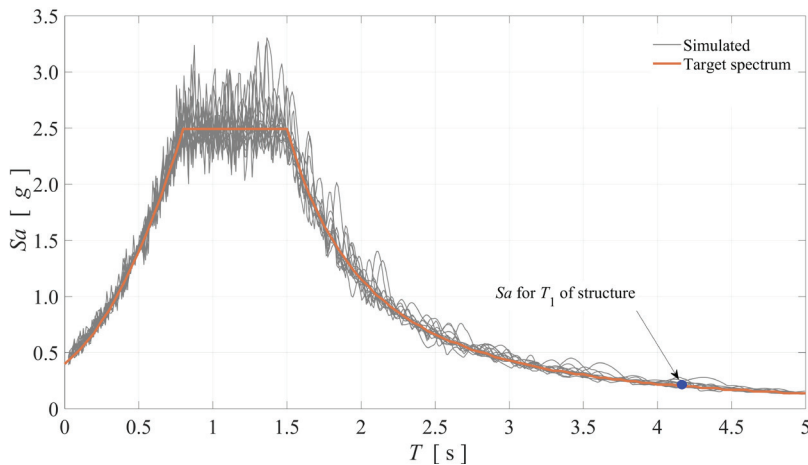


Figure 4. Acceleration response spectra from simulated records, PGA=0.4g

DAMAGE STATES DEFINITION

The defined damage thresholds consider diverse demand levels that could represent the performance of a non-habited structure, such as the one being analyzed. The first damage threshold is associated with a serviceability limit state, assuming the cracking or fallout of any of the quartz panels that compose the faces of the monument. Unfortunately, no information or document related to cracking- or fallout-mechanism to this specific material, or its placement configuration, has been found in the literature examination performed by the authors. Thus, it is assumed that this threshold is reached once the fallout drift limit, as defined in ASCE 7 (2022), has been reached. According to ASCE 7-22, the fallout limit for glazed curtain walls must satisfy the following relation:

$$\Delta_{\text{fallout}} \geq 1.25 D_{pl} \quad (3)$$

Where D_{pl} is a relative displacement defined as $D_{pl} = D_p I_e$ where I_e is the importance factor (assumed as 1 in this work), and $D_p = \Delta_{i+1} - \Delta_i$ where the drift Δ_i is defined between $0.010 h_i$ and $0.020 h_i$ for structures other than masonry, and h_i is the storey height bellow the level i . A value of $0.020 h_i$ is assumed for the present study. Thus, the damage threshold used in this work is defined as:

$$\Delta_{\text{fallout}} = 0.025 (h_{i+1} - h_i) \quad (4)$$

Where h_i and h_{i+1} are the height at level i and $i+1$, respectively. That is, it is being assumed that the damage state has been reached when the relative displacement between the two superior and inferior nodes of a selected structural element exceeds the value of Δ_{fallout} as defined above. It is worth mentioning that this criterion might be primarily associated to in-plane deformations of

curtain-wall facades, while the problem in hand might be mainly associated to out-of-plane deformation. Nonetheless, there is scarce information available on criteria for the latter in current design standards.

The second damage state corresponds to the yielding of one of the connecting beams between the two faces of the monument. Thus, the damage threshold selected for the evaluation of this damage state will be:

$$M_b \geq M_y = F_y S_x \quad (5)$$

Where M_b is the bending moment around the mayor axis of the beam cross-section, F_y the yielding stress of the material, assumed as 450 MPa, and S_x is the elastic section modulus of the beam around its mayor axis.

The last damage state defined corresponds to the failure of the main structural elements at the base of the monument. For this state the damage threshold has been defined as the element reaching its nominal capacity, defined as follows (ANSI/AISC 360, 2016):

$$\frac{P_r}{2P_c} + \left(\frac{M_{rx}}{M_{cx}} + \frac{M_{ry}}{M_{cy}} \right) \geq 1 \quad (6)$$

Where P_r , M_{rx} and M_{ry} are the axial force, bending moment in the x and y direction, respectively, and M_{cx} and M_{cy} are the capacity moments of the element around the local x and y axis, respectively, and P_c is the axial strength of the element, defined as (ANSI/AISC 360, 2016):

$$P_c = \left(0.658 \frac{F_y (L_c / r_x)^2}{\pi^2 E} \right) F_y A_g \quad (7)$$

Where E is the elastic modulus of the material, assumed as 2.01 GPa, r_x is the radius of gyration of the cross section around its mayor axis, L_c the effective length of the member, and A_g is the net area of the cross section. The bending strength of the element is defined as in damage state two, but with the plastic modulus corresponding to the column elements. Table 2 summarizes the damages states defined, as well as the thresholds associated of each of them.

CHARACTERIZATION OF PEAK STRUCTURAL RESPONSES

Response signals were obtained from the time-history analyses as described in Section Wind and seismic mathematical modeling. The maxima from these values were measured for each analysis, and their values were accounted for the determination of the probability of exceeding the damage thresholds and the influence of the TMDs on it. Figure 5 displays two comparisons for displacement at the top of the structure. One for wind-induced displacement under a wind intensity of 30 m/s, and another for earthquake-induced displacement with PGA of 0.4 g. The effects of the TMDs on the response maxima can be clearly appreciated; however, a quantification of these effects on the structural fragility is performed as described in the following paragraphs.

The probability distribution of the response maxima was checked for every level of intensity analyzed, so it could be ensured that the probability of failure is properly estimated (Martín del Campo & Pozos, 2019; Lima *et al.*, 2019). In the present study, the lognormal probability distribution was found to represent better the mean value of the structural response in the majority of cases. Thus, fragility could be evaluated with the common fragility expression:

$$F_i(IM) = \Phi \left[\frac{\ln \widehat{DP} - \ln dt_l}{\sigma_{\ln DP_l}} \right] \tag{8}$$

Where \widehat{DP} represents the median of the structural response or demand parameter employed for the evaluation of fragility, dt_l is the damage threshold for the l -th damage state, and $\sigma_{\ln DP_l}$ is the standard deviation of the natural logarithm of the demand parameter. IM is the intensity measure governing the demands on the structure, i.e. PGA, in the case of the earthquake action, or U_{10} when wind action is being evaluated. It is noted that only the uncertainty in the loads on the structure is considered. The inclusion of uncertainty in the structural properties and characteristics is out of the scope of the present study.

Table 2. Damage states defined for fragility analysis

Damage State	Threshold	Description
DS_1	$0.0125 (h_{i+1} - h_i)$	Cracking or fallout of quartz panel. Relative displacement is exceeded
DS_2	M_y	Bending moment of connection beams exceeds yielding moment
DS_3	$\frac{P}{2P_c} + \left(\frac{M_{rx}}{M_{cx}} + \frac{M_{ry}}{M_{cy}} \right)$	The design capacity of the main supporting columns is reached

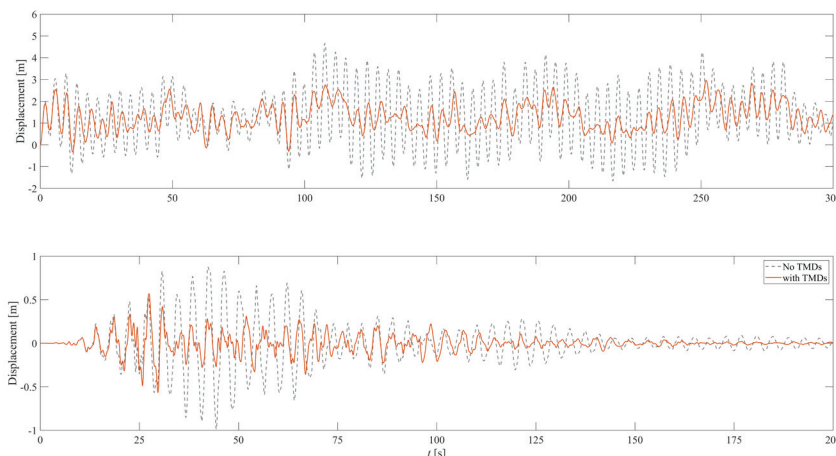


Figure 5. Response-history comparison for wind (top) and earthquake (bottom)

The fragility can be estimated from a continuous function if an expression describing the median demand parameter is defined. Thus, a regression analysis on the results was performed to define such a function. This criterion also allows to define the uncertainty associated with the demand on the structure, by measuring $\sigma_{\ln DP_i}$ from the residuals of the regression (Martín del Campo *et al.*, 2021).

Exponential functional models, with the form $y = a \exp(bx)$, were found to represent well the tendencies of the majority of structural responses studied in the analyses, whereas a linear model with form $y = ax + b$ suited better for DS_3 for the earthquake cases. Table 3 summarizes the models used to represent the response maxima, as well as their coefficients and values of $\sigma_{\ln DP_i}$.

Figures 6a and 6b show the fitted expressions found to represent the median of the response maxima for every wind intensity level and damage states analyzed, for the with- and without-TMD cases. The uncertainty from each model is reported in Table 3. Lesser uncertainty is found in most cases of the structures analyzed with TMDs, this is justified in the reduction of the root mean square (RMS) value of the structural response

when the structure is fitted with TMDs (Martín del Campo *et al.*, 2021). Analogously, the regression models are presented for the with- and without-TMD analyses under earthquake action in Figures 7a and 7b.

The evaluation of fragility under multiple hazards can be performed similarly as the single-hazard case. For that purpose, an expression describing the mean of the demand parameter is defined as function of the involved intensities, as well as the variation of its standard deviation. For the cases analyzed in this work, a function with the form $\widehat{DP} = a_1 IM_1^{b_1} + c_1 IM_2^{d_1}$ was found adequate to describe the median of the demand parameter for each damage state, where IM_1 represents the earthquake intensity as a fraction of g , and IM_2 represents the mean wind velocity normalized by the maximum mean velocity considered, i.e., $U_{10}/60$ (in m/s). As for the standard deviation of the demands on the structure, a function with the form of $\sigma = a_2 IM_1 + b_2 IM_2^{c_2} + d_2$ defined adequately the dispersion of the data.

Table 4 lists the values of the coefficients obtained for each of the damage states, for the damped and undamped cases.

Table 3. Summary of response-models and their parameters

Structural Case	Load Case	DS	Form ¹	$\ln a$	b	$\sigma_{\ln DP}$
No TMD	Wind	1	e	-4.755	0.167	0.109
		2	e	12.840	0.075	0.110
		3	e	-4.084	0.055	0.311
	Earthquake	1	e	-3.839	7.299	0.087
		2	e	14.150	2.059	0.067
		3	l	-1.307	0.004	0.061
TMD	Wind	1	e	-4.834	0.160	0.120
		2	e	12.720	0.073	0.090
		3	e	-4.223	0.052	0.277
	Earthquake	1	e	-4.043	7.211	0.088
		2	e	14.020	2.154	0.067
		3	l	-1.358	0.001	0.057

Notes: 1) e = exponential; l = lineal

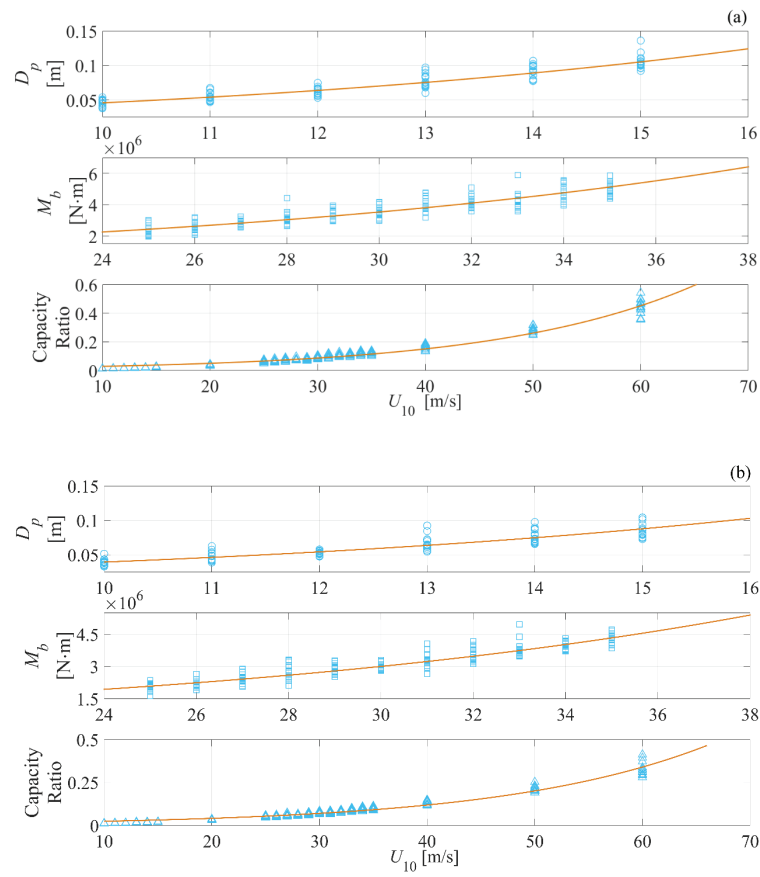


Figure 6. Maxima of structural responses for wind: (a) without TMDs; (b) with TMDs

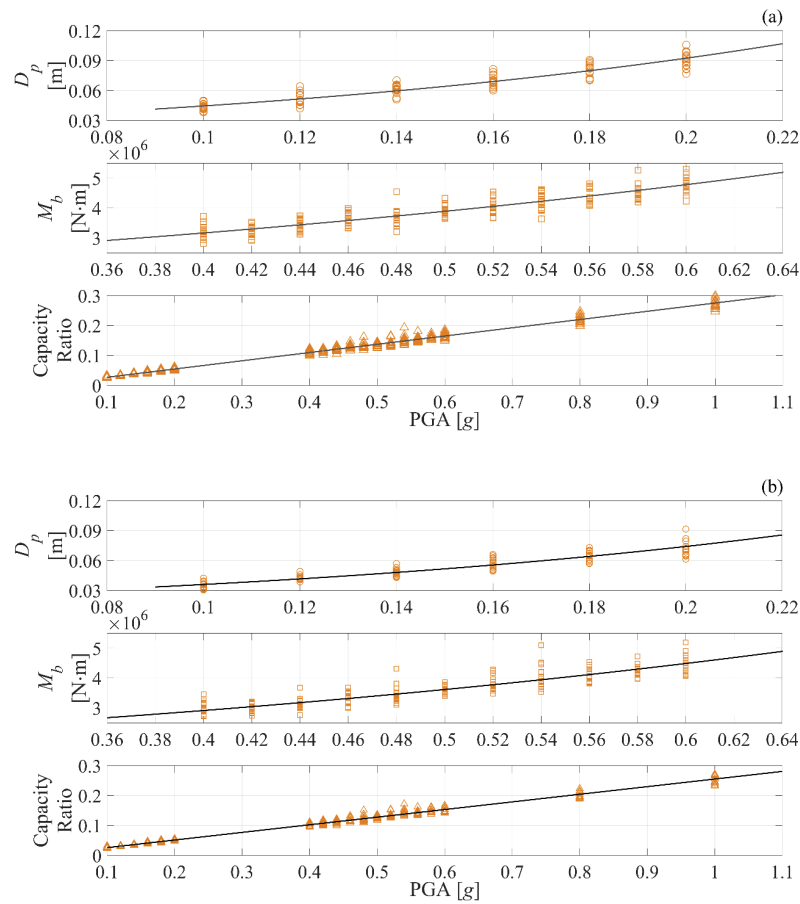


Figure 7. Maxima of structural responses for earthquake: (a) without TMDs; (b) with TMDs

Table 4. Coefficients for multi-hazard models

	No TMDs			With TMDs		
	DS_1	DS_2	DS_3	DS_1	DS_2	DS_3
a_1	2.260	1.648	0.241	1.894	1.550	0.234
b_1	0.590	0.838	0.806	0.655	0.853	0.851
c_1	18.762	3.537	0.331	12.758	2.697	0.226
d_1	2.590	2.667	3.068	2.419	2.547	2.853
a_2	0.179	0.110	0.014	0.089	0.123	0.013
b_2	2.817	0.568	0.047	1.276	0.338	0.033
c_2	3.709	3.871	3.320	1.993	2.708	2.879
d_2	0.191	0.038	0.003	0.015	0.003	0.001

ANALYSIS RESULTS

FRAGILITY CURVES FOR SINGLE HAZARD

The evaluation of fragility on the structures was performed according to the criteria described above. As expected, a higher probability of damage is found from wind action than from earthquake, since the dynamic properties of the structure place its fundamental period far from the plateau of the seismic spectra. Furthermore, a relatively small probability of failure is found for DS_3 , which is completely negligible in the earthquake cases. Figures 8 and 9 show the fragility functions for wind and earthquake action, respectively, as well as the reliability enhancement (ΔF) achieved with the use of the passive dampers. ΔF is computed as the subtraction of the fragility values considering the TMDs on the structure, to their respective probability of failure without TMDs (Martín del Campo *et al.*, 2021).

The greatest reliability enhancement is found under earthquake action for DS_1 , which implies a reduction of nearly 80 % in the probability of failure for PGA values of $\sim 0.15g$. This value is inferior to the acceleration ordinate for zero seconds presented in the design spectrum

according to NTC-DS (2020). For wind action on the structure, observing the same damage state, the reduction in the probability of failure is subtly greater than 50 % for a wind speed of ~ 13 m/s, which is slightly superior to the design speed proposed by NTC-DV (2017) for a structure with high level of importance.

For DS_2 , greater enhancement in probability of failure is seen for wind action than for earthquake. Values of nearly 60 % lesser probability of failure are seen at wind intensities of ~ 32 m/s when TMDs are installed on the structure, while ~ 40 % less probability of failure is seen for earthquake action at PGA values near 0.5 g.

In all cases, the use of TMDs reduces the probability of exceedance ($F(U_{10})$ or $F(PGA)$) given any of the damage states considered with respect to the structure without TMDs for the same intensity level (U_{10} or PGA). As already mentioned, the greater reduction of fragility among the three damage states is seen for earthquake action. However, since the structure is a flexible system, these improvements in fragility are seen at high ground-motion intensities, whereas the enhancement in fragility for wind action is seen at a wider range of the covered intensities.

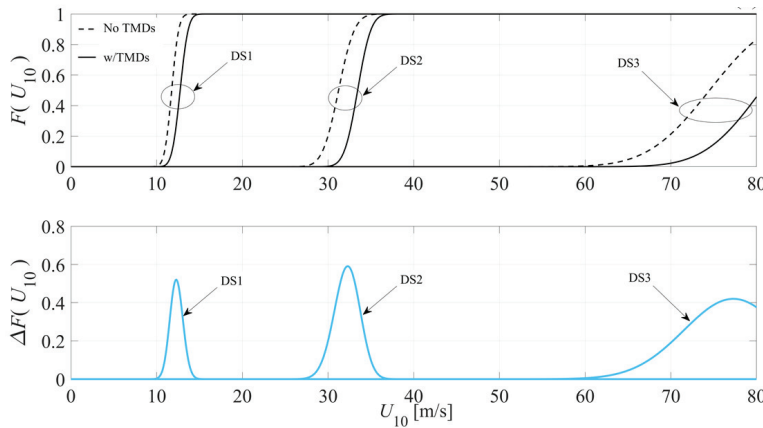


Figure 8. Fragility evaluation for wind action on the structure

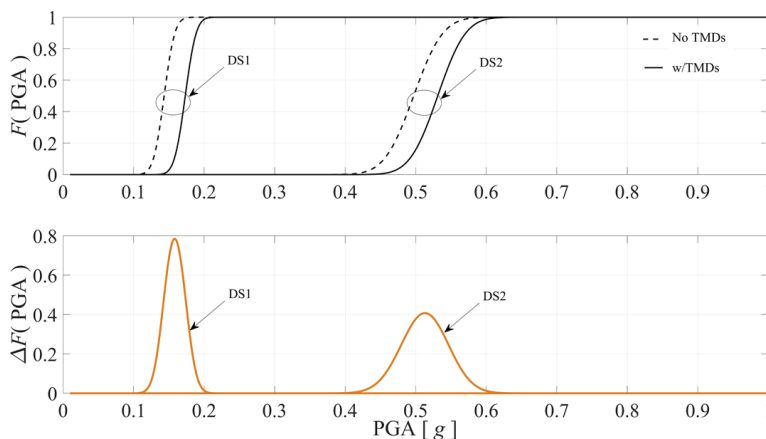


Figure 9. Fragility evaluation for earthquake action on the structure

FRAGILITY CURVES FOR MULTIPLE HAZARD

It is observed in Figures 10 to 12 that the use of TMDs for multiple hazard reduces the probability of exceedance given any of the damage states considered, the amount of reduction depends on the intensity measure and the damage state evaluated. Figure 10 indicates that, for DS_1 , the structure with TMDs installed is more effective at reducing the fragility values under high wind effects for low levels of PGA; however, the use of TMDs is less effective for low levels of wind loading and moderate levels of PGA. For DS_2 , it is observed in Figure 11 an increase in the effectiveness of the use of TMDs for PGA values above 0.5g and low values of wind speed, this effectiveness increases as the wind

speed increases and the PGA reduces. Figure 12 shows that for DS_3 , the fragility values are almost independent of the PGA, which indicates that the probability of exceeding the design capacity of the main supporting columns is very low. It is also observed in Figure 12 that the use of TMDs is less effective for wind speed values above 90 m/s.

A comparison of the reliability enhancement for multiple hazard indicates that, in general, the TMDs are more effective at reducing the possible damages due to cracking or fallout of quartz panels and the yielding of connection beams due to bending moment. This observation is advantageous since the use of an optimal TMD system can effectively reduce different structural responses with similar effectiveness.

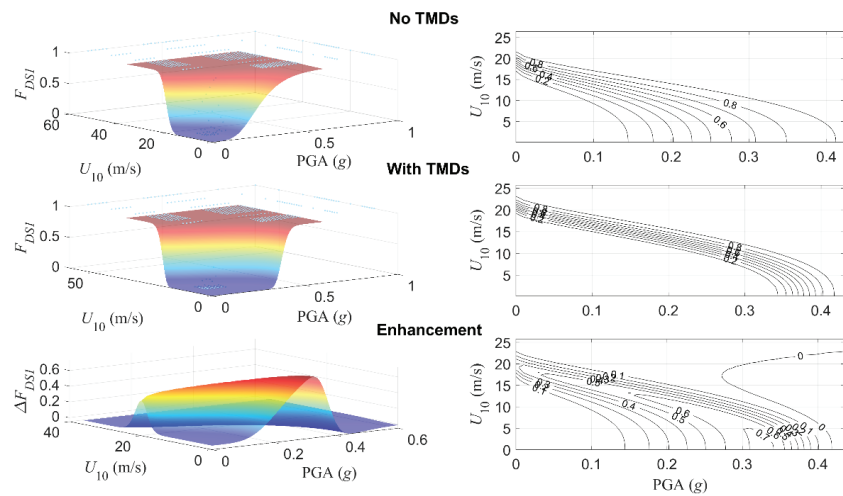


Figure 10. Fragility surfaces and fragility enhancement for DS_1

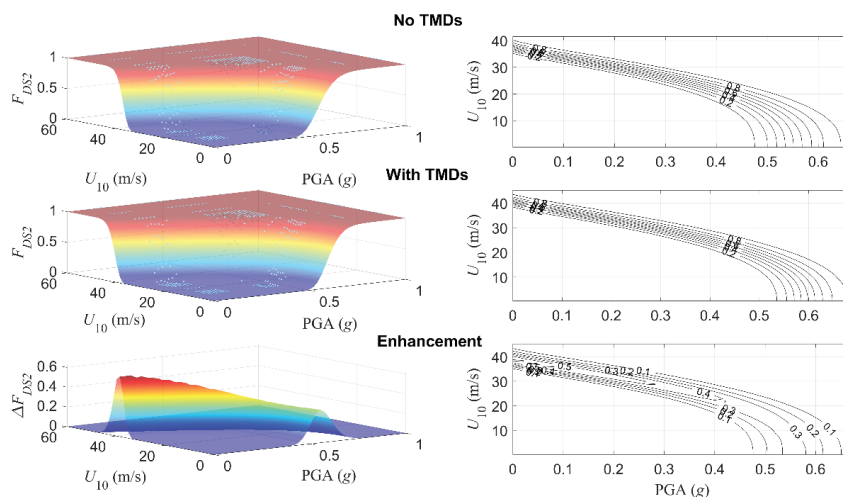


Figure 11. Fragility surfaces and fragility enhancement for DS_2

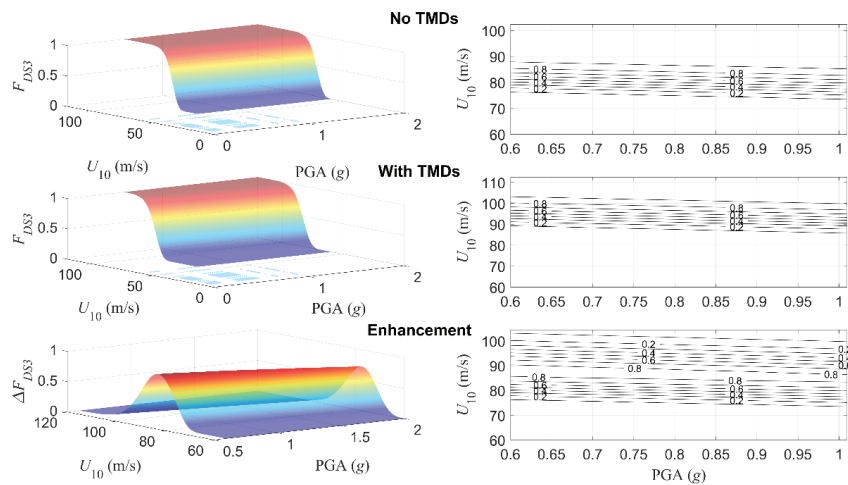


Figure 12. Fragility surfaces and fragility enhancement for DS_3

CONCLUSIONS

A numerical study of a slender monument structure fitted with TMDs was performed to develop fragility curves and surfaces, considering turbulent wind and seismic loading alone and simultaneously. The damage states considered for the fragility analysis are associated to different performance levels of the structure, based on criteria established in common normative for civil structures. For the studied structure, the developed fragility functions allowed to evaluate the structural performance without and with the use of a TMD system by considering fragility enhancement. It must be emphasized that the present study accounts for simulated wind and ground-motion records. This was performed due to the unavailability of using records from both hazards in a range of intensity levels as wide as the one used in the present study. Notwithstanding, since the criteria adopted for their simulation follows conventions accepted in the literature, the implications of their use can be limited to the variability observed in the studied phenomena. Moreover, the damage states selected for the fragility analysis are non-correspondent to monument structures, which implies that this can be an area of opportunity for other studies of such kind of structures.

Notwithstanding the commented limitations from the present study, the analysis results indicated that for single and multiple hazards, the use of TMDs reduces the probability of failure for all damage states considered, with respect to the structure without TMDs for the same intensity levels (U_{10} or PGA). More specifically, it is concluded that:

1) For the structure considered, a higher probability of damage is found from wind action than from ear-

thquake. An important reliability enhancement is achieved with the use of TMDs. A relatively small probability of failure is found for DS_3 , which is completely negligible in the earthquake cases.

- 2) The greatest reliability enhancement is found under earthquake action for DS_1 , which implies a reduction of nearly 80 % in the probability of failure for PGA values of ~ 0.15 g. For wind action on the structure, observing the same damage state, the reduction in the probability of failure is slightly greater than 50 % for a wind speed of about 13 m/s.
- 3) The most notorious impact of the use of TMDs is the reduction of the fragility values under wind effects and low levels of PGA for DS_1 . This reduction on the fragility values changes when DS_2 is considered, where an increase in the effectiveness of using TMDs for PGA values above 0.5g and low values of wind speed is observed.
- 4) For DS_3 , the fragility values are almost independent of the PGA, which indicates that the probability of exceeding the design capacity of the main supporting columns is very low.

ACKNOWLEDGEMENTS

We are grateful for the financial support from the Mexican National Council for Science and Technology (CONACyT) and the Institute of Engineering of UNAM (II-UNAM). We also thank DGAPA PAPIIT project IN103422 for the financial support provided.

REFERENCES

ANSI, A. (2016). 360-16. Specification for structural steel buildings american institute of steel construction.

- ANSYS® Academic Research Mechanical, Release 19.0. (2019). ANSYS Parametric Design Language Analysis Guide, ANSYS, Inc
- Asareh, M. A., Schonberg, W., & Volz, J. (2016). Fragility analysis of a 5-MW NREL wind turbine considering aero-elastic and seismic interaction using finite element method. *Finite Elements in Analysis and Design*, 120, 57-67. <https://doi.org/10.1016/j.finel.2016.06.006>
- ASCE American Society of Civil Engineers. (2022). Minimum design loads for buildings and other structures, ASCE/SEI 7-22, ASCE, Reston, Virginia
- Casciati, S., & Faravelli, L. (2010). Vulnerability assessment for medieval civic towers, *Structure and Infrastructure Engineering*, 6(1-2), 193-203. <https://doi.org/10.1080/15732470802664290>
- Comisión Federal de Electricidad (2020). Manual de diseño de obras civiles. Diseño por viento, Instituto Nacional de Electricidad y Energías Limpias, Ciudad de México.
- Cui, W., Ma, T., & Caracoglia, L. (2020). Time-cost "trade-off" analysis for wind-induced inhabitability of tall buildings equipped with tuned mass dampers. *Journal of Wind Engineering & Industrial Aerodynamics*, 207, 104394. <https://doi.org/10.1016/j.jweia.2020.104394>
- Davenport, A. G. (1968). *Proceedings of the international research seminar on wind effects on buildings and structures*. Toronto: University of Toronto Press.
- Engineering Sciences Data Unit: (1975). Characteristics of atmospheric turbulence near the ground, Part III', ESDU Item 75001, Regent St., London, 27 pp.
- García, A. D., Pozos, A., Gómez, R., & Hong, H. P. (2012). Peligro sísmico debido a sismos interplaca e inslab y su impacto en el diseño. *Revista de Ingeniería Sísmica*, 86, 27-54. (In Spanish).
- Gioffre, M., Gusella, V., & Cluni, F. (2008). Performance evaluation of monumental bridges: testing and monitoring 'Ponte delle Torri' in Spoleto. *Structure and Infrastructure Engineering*, 4(2), 95-106. <https://doi.org/10.1080/15732470601155300>
- Hong, H. P., & Liu, T. J. (2014). Assessment of coherency for bidirectional horizontal ground motions and its application for simulating records at multiple stations. *Bulletin of the Seismological Society of America*, 104(5), 2491-2502. <https://doi.org/10.1785/0120130241>
- Hong, H. P., & Liu, T. J. (2017). Site, local, and regional earthquake ground motion characterization and application. *Advances in Structural Engineering*, 20(1), 34-50. <https://doi.org/10.1177/2F1369433216646004>
- Hong, H. P., & Cui, X. Z. (2020). Time-frequency spectral representation models to simulate nonstationary processes and their use to generate ground motions. *J. Eng. Mech.* 146(9), 04020106. [https://doi.org/10.1061/\(ASCE\)EM.1943-7889.0001827](https://doi.org/10.1061/(ASCE)EM.1943-7889.0001827)
- Jaimés, M. A., García, A. D., Martín del Campo, J. O., & Pozos, A. (2020). Probabilistic risk assessment on wind turbine towers subjected to cyclone-induced wind loads. *Wind Energy*, 23(3), 528-546. <https://doi.org/10.1002/we.2436>
- Kaimal, J. C., Wyngaard, J. C. J., Izumi, Y., & Coté, O. R. (1972). Spectral characteristics of surface-layer turbulence. *Quarterly Journal of the Royal Meteorological Society*, 98(417), 563-589. <https://doi.org/10.1002/qj.49709841707>
- Li, H. N., Liu, Y., Li, C., & Zheng, X. W. (2020). Multihazard fragility assessment of steel-concrete composite frame structures with buckling-restrained braces subjected to combined earthquake and wind. *The Structural Design of Tall and Special Buildings*, 29(11), e1746. <https://doi.org/10.1002/tal.1746>
- Lima, I. F., Gómez, R., & Pozos, A. (2019). Methodology to develop fragility curves of glass façades under wind-induced pressure. *International Journal of Civil Engineering*, 17(3), 347-359. <https://doi.org/10.1007/s40999-018-0360-6>
- Liu, T. J., & Hong, H. P. (2015). Simulation of horizontal ground motions with spatial coherency in two orthogonal horizontal directions. *Journal of Earthquake Engineering*, 19(5), 752-769. <https://doi.org/10.1080/13632469.2014.999175>
- Martin del Campo, J. O., & Pozos, A. (2019). Multi-hazard fragility analysis for a wind turbine support structure: an application to the Southwest of Mexico. *Engineering Structures*. 209, 109929. <https://doi.org/10.1016/j.engstruct.2019.109929>
- Martin del Campo, J. O., Pozos, A., & Pozos, O. (2021). Development of fragility curves of land-based wind turbines with tuned mass dampers under cyclone and seismic loading. *Wind Energy*, 24(7), 737-753. <https://doi.org/10.1002/we.2600>
- NTC-Sismo, Normas Técnicas Complementarias para Diseño por Sismo. (2020). Reglamento de Construcciones de la Ciudad de México, Gaceta Oficial de la Ciudad de México.
- NTC-Viento, Normas Técnicas Complementarias para Diseño por Viento. (2017). Reglamento de Construcciones de la Ciudad de México, Gaceta Oficial de la Ciudad de México.
- Padgett, J. E., & DesRoches, R. (2009). Retrofitted bridge fragility analysis for typical classes of multispan bridges. *Earthquake Spectra*, 25(1), 117-141. <https://doi.org/10.1193/2F1.3049405>
- Pozos, A., & Hong, H. P. (2015). Sensitivity analysis of the effectiveness of tuned mass dampers to reduce the wind-induced torsional responses. *Latin American Journal of Solids and Structures*, 12, 250-2538.
- Pozos, A., & Gómez, R. (2019). Parametric study of the use and optimization of tuned mass dampers to control the wind-and seismic-induced responses of a slender monument. *The Structural Design of Tall and Special Buildings*, 28(13), e1633. <https://doi.org/10.1002/tal.1633>
- Pozos, A., Gómez, R., & Hong, H. (2014). Desagregación del peligro sísmico para algunos sitios seleccionados de México. *Ingeniería sísmica. Revista de Ingeniería Sísmica*, (91), 31-53. (In Spanish).
- Pozos, A., Liu, T. J., Gomez, R., & Hong, H. P. (2016). Seismic design and importance factor: benefit/cost for overall service time versus per unit service time. *Structural Safety*, 58, 40-51. <https://doi.org/10.1016/j.strusafe.2015.08.005>

- Vanmarcke, E. A., & Gasparini, D. A. (1976). *A program for artificial motion generation-User's manual and documentation*. Cambridge, M. A.: Department of Civil Engineering, MIT.
- Wong, K. K., & Harris, J. L. (2012). Seismic damage and fragility analysis of structures with tuned mass dampers based on plastic energy. *The Structural Design of Tall and Special Buildings*, 21(4), 296-310. <https://doi.org/10.1002/tal.604>
- Zhang, W., Liu, S., Mehrdad, S., Ahmad, D., & Ertugrul, T. (2022). Nonlinear seismic fragility assessment of tall buildings equipped with tuned mass damper (TMD) and considering soil-structure interaction effects. *Bulletin of Earthquake Engineering*, 20, 3469-3483. <https://doi.org/10.1007/s10518-022-01363-6>
- Zhao, B., Gao, H., Wang, Z., & Lu, Z. (2018). Shaking table test on vibration control effects of a monopile offshore wind turbine with a tuned mass damper. *Wind Energy*, 21(12), 1309-1328. <https://doi.org/10.1002/we.2256>
- Zheng, X. W., Li, H. N., Yang, Y. B., Li, G., Huo, L. S., & Liu, Y. (2019). Damage risk assessment of a high-rise building against multihazard of earthquake and strong wind with recorded data. *Engineering Structures*, 200, 109697. <https://doi.org/10.1016/j.engstruct.2019.109697>
- Zhou, C., Zeng, X., Pan, Q., & Liu, B. (2015). Seismic fragility assessment of a tall reinforced concrete chimney. *The Structural Design of Tall and Special Buildings*, 24(6), 440-460. <https://doi.org/10.1002/tal.1173>

Cómo citar:

Pozos-Estrada, A., Martin del Campo-Preciado, J. O., & Pozos-Estrada, O. (2024). Fragility curves of a slender structure fitted with tuned mass dampers subjected to turbulent wind and seismic loading. *Ingeniería Investigación y Tecnología*, 25 (04), 1-15. <https://doi.org/10.22201/fi.25940732e.2024.25.4.027>